Periodic Handover Skipping in Cellular Networks: Spatially Stochastic Modeling and Analysis

Kiichi Tokuyama, Tatsuaki Kimura, and Naoto Miyoshi

Abstract

Handover (HO) management is one of the most crucial tasks in dense cellular networks with mobile users. A problem in the HO management is to deal with increasing HOs due to network densification in the 5G evolution and various HO skipping techniques have so far been studied in the literature to suppress excessive HOs. In this paper, we propose yet another HO skipping scheme, called *periodic HO skipping*. The proposed scheme prohibits the HOs of a mobile user equipment (UE) for a certain period of time, referred to as skipping period, thereby enabling flexible operation of the HO skipping by adjusting the length of the skipping period. We investigate the performance of the proposed scheme on the basis of stochastic geometry. Specifically, we derive analytical expressions of two performance metrics—the HO rate and the expected downlink data rate—when a UE adopts the periodic HO skipping. Numerical results based on the analysis demonstrate that the periodic HO skipping scenario can outperform the scenario without any HO skipping in terms of a certain utility metric representing the trade-off between the HO rate and the expected downlink data rate, in particular when the UE moves fast. Furthermore, we numerically show that there can exist an optimal length of the skipping period, which locally maximizes the utility metric, and approximately provide the optimal skipping period in a simple form. Numerical comparison with some other HO skipping techniques is also conducted.

Index Terms

This work has been presented in part in [1].

K. Tokuyama and N. Miyoshi are with the Department of Mathematical and Computing Science, Tokyo Institute of Technology, Tokyo, Japan. E-mail: tokuyama.k.aa@m.titech.ac.jp, and miyoshi@is.titech.ac.jp. T. Kimura is with the Department of Information and Communications Technology, Osaka University, Osaka, Japan. E-mail: kimura@comm.eng.osaka-u.ac.jp.

This work was supported by the Japan Society for the Promotion of Science (JSPS) Grant-in-Aid for Scientific Research (C) 19K11838.

Cellular networks, mobility, handover skipping, handover rate, data rate, stochastic geometry.

I. Introduction

The development of the fifth generation mobile communication systems (5G) is driven by the ever-increasing demand for channel capacity due to the proliferation of mobile user equipments (UEs) such as mobile phones, tablets, and other handheld devices. One of the key solutions in the 5G evolution is network densification through small cell deployments (see, e.g., [2], [3]). Densifying base stations (BSs) offers more capacity, which improves the quality of service. On the other hand, it shrinks the service area of each BS and induces frequent handovers (HOs), which may increase the signaling overhead and the risk of disconnections.

HO skipping is an approach to address the problem of frequent HOs by skipping some opportunities of HOs (see, e.g., [4]–[10]). However, in turn, the HO skipping may decrease the data reception rate (data rate for short) since it tends to force a UE to retain long-distance connection with a BS. In other words, the HO skipping induces a trade-off between the HO rate and the data rate, and this trade-off should be balanced for the network densification to work effectively. While various HO skipping techniques have so far been proposed and studied in such a point of view, we propose yet another HO skipping scheme, called *periodic HO skipping*. The proposed scheme prohibits the HOs of a mobile UE for a certain period of time, referred to as *skipping period*, thereby enabling flexible operation of the HO skipping by adjusting the length of the skipping period. In this paper, we investigate the performance of the proposed scheme from the perspective of the trade-off between the HO rate and the data rate.

A. Related Work

A number of studies have so far analyzed the performance of cellular networks with mobile UEs and many of them have adopted stochastic geometry as an analytical tool (see, e.g., recent tutorial articles [11], [12] and references therein). In the stochastic geometry approach, the locations of wireless nodes (BSs and/or UEs) in a wireless network are modeled by stochastic point processes on the Euclidean plane, so that we can capture the spatial irregularity of wireless nodes and explore mathematical analysis of region-independent network performance by virtue of the theory of point processes and stochastic geometry. The first results along this line date back to the late 1990s [13], [14], where the cells associated with BSs in a cellular network are modeled as the Voronoi tessellation formed by a homogeneous Poisson point process (PPP) and some performance metrics concerning mobile UEs are discussed. Since the 2010s, this stream has become more active. Lin *et al.* [15] propose a mobility model of a UE on single-tier hexagonal/PPP networks and analyze the HO rate and the expected sojourn time of a mobile UE staying in a particular cell. The results in [15] are then extended in [16] to a two-tier heterogeneous network (HetNet). Bao and Liang [17] derive an analytical expression for the HO rate in a multi-tier HetNet modeled using overlaid independent PPPs and provide a guideline for tier selection taking both the HO rate and the expected downlink data rate into account. In addition, [18] develops a similar analysis to [17] for a single-tier network with BS cooperation. Sadr and Adve [19] analyze the HO rate in a PPP model of multi-tier HetNets with orthogonal spectrum allocation among tiers and investigate the negative impact of HOs on the coverage probability. Chattopadhyay *et al.* [20] evaluate the expected downlink data rate for a mobile UE taking into account the data outage periods due to HOs in a two-tier HetNet and further discuss the fraction of connecting BSs to reduce frequent HOs.

Several HO skipping techniques have also been proposed and analyzed using the stochastic geometry (see, e.g., [4]–[8]). Arshad *et al.* [4] introduce the so-called alternate HO skipping, where a mobile UE executes HOs alternately along its trajectory, and quantify the average throughput representing the trade-off between the HO rate and the expected downlink data rate when a UE adopts the alternate HO skipping. The results in [4] are extended in [5] to a two-tier HetNet and in [6] to the incorporation with BS cooperation. Furthermore, [7] proposes topology-aware HO skipping, where a UE skips an HO when the target BS is far from the UE's trajectory or the cell of the target BS is small, and evaluates its performance by Monte Carlo simulations. Demarchou *et al.* [8] then provide a mathematical analysis of the topology-aware HO skipping. Compared with these sophisticated HO skipping techniques, our proposed scheme is simple and easy to implement since it is enough for a mobile UE to observe the BS locations every fixed-length period (as seen in the definition of the scheme in Sec. II-B). We will find later that such a simple scheme can compete with the sophisticated ones.

B. Contributions

The contributions of this work are summarized as follows.

1) We propose and advocate the periodic HO skipping, which prohibits the HOs of a mobile UE during each cycle of the skipping period.

2) Applying the stochastic geometry approach, we derive the analytical expressions of the HO rate and the expected downlink data rate when a mobile UE adopts the periodic HO skipping.
3) On the basis of the analytical results, we numerically demonstrate that the proposed scheme can outperform the conventional scenario without any HO skipping, in particular when the UE moves fast.
4) We numerically observe that there can exist an optimal length of the skipping period and provide an approximate optimal skipping period in a simple computable form.
5) We numerically observe that the proposed scheme can compete with some other sophisticated HO skipping techniques.

This work enhances [1], where the periodic HO skipping is already proposed. However, the contributions in analysis 2) and the numerical experiments 3) are fundamentally refined. Moreover, the contributions 4) and 5) are completely new.

C. Organization

The rest of the paper is organized as follows. In the next section, we describe the network model and our proposed periodic HO skipping scheme. We then define the user mobility model and the performance metrics; that is, the expected downlink data rate and the HO rate. In Sec. III, the performance of the proposed scheme is investigated, where for comparison, we analyze the performance metrics not only for the proposed scheme but also for the scenario without any HO skipping. Then, on the basis of the analytical results, the performances of the two scenarios are numerically compared in terms of a certain utility metric representing the trade-off between the data rate and the HO rate. In Sec. IV, we discuss how to decide the length of the skipping period, where we numerically observe that there exists an optimal length of the skipping period which locally maximizes the utility metric. We then provide a simple computable expression of an approximate optimal skipping period. Some properties of the approximate optimal skipping period are also revealed by numerical experiments. Numerical comparison with some other HO skipping techniques are made in Sec. V. Finally, the paper is concluded in Sec. VI.

II. System Model and Periodic Handover Skipping

A. Network Model

In this paper, we develop our proposed periodic HO skipping scheme implemented on the most basic spatially stochastic model of cellular networks; that is, a homogeneous PPP network with Rayleigh fading and power-law path-loss (see, e.g., [21], [22]). Before defining the proposed scheme, we detail here the network model.

BSs in a cellular network are deployed according to a homogeneous PPP $\Phi = \sum_{i\in\mathbb{N}} \delta_{X_i}$ on the Euclidean plane $\mathbb{R}^2$ with intensity $\lambda \in (0, \infty)$, where $\mathbb{N} := \{1, 2, \ldots\}$, δ_x denotes the Dirac measure with mass at $x \in \mathbb{R}^2$ and the points $X_1, X_2, \ldots$ of Φ are numbered in an arbitrary order. All the BSs transmit signals with the same power level, normalized to one, using a common spectrum bandwidth. We suppose that the time is divided into discrete slots and the downlink channels are affected by Rayleigh fading and power-law path-loss, whereas shadowing effects are ignored. Therefore, if a UE located at $\boldsymbol{u} \in \mathbb{R}^2$ at slot $t \in \mathbb{N}_0 := \mathbb{N} \cup \{0\}$ receives a signal from the BS at X_i, $i \in \mathbb{N}$, the received signal power is represented by $H_{i,t}\|X_i - \boldsymbol{u}\|^{-\beta}$, where $\|\cdot\|$ stands for the Euclidean norm, $H_{i,t}$, $i \in \mathbb{N}$, $t \in \mathbb{N}_0$, are mutually independent and exponentially distributed random variables with unit mean representing the fading effects, and $\beta > 2$ denotes the path-loss exponent.

We assume that, at any time slot, each BS has at least one UE in service and transmits a signal to one of its UEs. Then, if a UE is located at $\boldsymbol{u} \in \mathbb{R}^2$ at slot $t \in \mathbb{N}_0$ and is served by the BS at X_i, the downlink signal-to-interference-plus-noise ratio (SINR) for this UE is represented by

$$\mathsf{SINR}_{\boldsymbol{u},i}(t) = \frac{H_{i,t}\|X_i - \boldsymbol{u}\|^{-\beta}}{I_{\boldsymbol{u},i}(t) + \sigma^2}, \quad i \in \mathbb{N},\ t \in \mathbb{N}_0, \tag{1}$$

where σ^2 denotes a nonnegative constant representing the noise power and $I_{\boldsymbol{u},i}(t)$ denotes the total interference power to this UE given by

$$I_{\boldsymbol{u},i}(t) = \sum_{j\in\mathbb{N}\setminus\{i\}} H_{j,t}\,\|X_j - \boldsymbol{u}\|^{-\beta}. \tag{2}$$

The instantaneous downlink data rate $\xi_{\boldsymbol{u},i}(t)$ is then defined as

$$\xi_{\boldsymbol{u},i}(t) = \log(1 + \mathsf{SINR}_{\boldsymbol{u},i}(t)), \tag{3}$$

where log stands for the natural logarithm for simplicity, but of course, it can be converted into the conventional binary logarithm by multiplying the constant $\log_2 e$.

B. Periodic Handover Skipping

Suppose that a UE moves on $\mathbb{R}^2$ and is initially (at slot 0) served by its nearest BS, which offers the strongest signal power to the UE when the fading effects are averaged out. In other words, the cells of respective BSs form a Poisson-Voronoi tessellation (see [23, Sec. 9.7]). In our proposed periodic HO skipping scheme, a UE is prohibited from executing HOs and retains the initial connection for s time slots, referred to as *skipping period*, regardless of its motion. After the skipping period of s slots has passed, the UE reexamines the connection and if the current connection is no longer with the nearest BS due to its moving, the UE executes an HO and makes a new connection with the nearest one. Afterward, this procedure is repeated in cycles of the skipping period. Namely, the UE reexamines its connection to a BS every s time slots, during which it skips any chances of HOs even if it crosses the boundaries between cells. We assume that an HO, if it is done, is executed instantly without any time loss. We should note that a UE is always connected to its nearest BS at the beginning of each cycle of the skipping period, whereas it does not always execute an HO at the end of a cycle since the current connection can still be with the nearest one.

One may claim that the skipping period described above is similar to the time-to-trigger (TTT) in Long-Term Evolution (LTE) [24]. Indeed, they both suppress the number of HOs by prohibiting them for a certain period of time. However, they are substantially different in that the TTT starts at the instant that a UE crosses a boundary between two cells and it is in the order of 100msec, which mainly aims to prevent ping-pong phenomena around the boundaries between cells. On the other hand, the skipping period repeats in cycles and prohibits HOs during each cycle, which is in the order of seconds (though it may depend on the speed of the UE).

Clearly, the choice of the length of the skipping period is vital for our proposed scheme. If the skipping period is too short, it results in frequent HOs, whereas the long skipping period may cause long-distance connections, which deteriorate the transmission performance. Therefore, we should decide the length of the skipping period carefully.

C. Mobility Model

Owing to the spatial stationarity of the network model, we can focus on a UE that is supposed to be at the origin $\mathbf{0} = (0, 0) \in \mathbb{R}^2$ at slot 0 and we refer to this UE as the *typical UE*. Let $S(t)$ denote the location of the typical UE at slot $t \in \mathbb{N}_0$. Since a UE is allowed to execute an HO every cycle of the skipping period in our proposed scheme, it is enough to observe the location

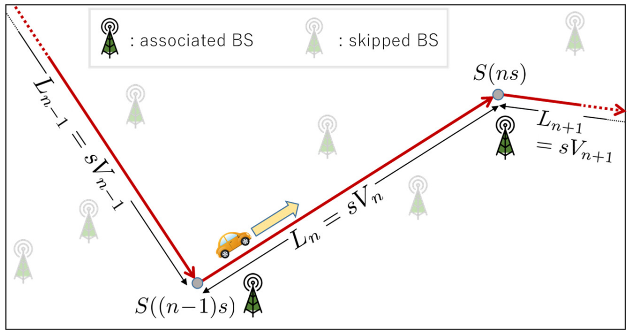

Fig. 1. A path of the typical UE in the random walk mobility model.

of the typical UE every cycle and we model its motion as a simple and tractable random walk on $\mathbb{R}^2$. Let $Y_1, Y_2, \dots$ denote a sequence of independent and identically distributed (i.i.d.) random variables on $\mathbb{R}^2$ representing the motions of the typical UE in respective cycles of the skipping period. Then, the location of the typical UE just after n cycles (that is, at slot ns) is provided as a random work;

$$S(ns) = \sum_{k=1}^{n} Y_k, \quad n \in \mathbb{N}, \tag{4}$$

with $S(0) = \mathbf{0}$. We assume that the typical UE moves along the straight line segment at a constant velocity during each cycle; that is, $\{S(t)\}_{t\in\mathbb{N}_0}$ is piecewise deterministic and is given by

$$S(t) = S(ns) + \frac{t - ns}{s} Y_{n+1}, \quad t = ns, ns+1, \dots, (n+1)s, \ n \in \mathbb{N}_0. \tag{5}$$

An example of a path of the typical UE is illustrated in Fig. 1. Let $Y_n = (L_n, \psi_n)$, $n \in \mathbb{N}$, in the polar coordinates. Then, the moving speed of the typical UE during the nth cycle is equal to $V_n = L_n/s$. It is reasonable to suppose that the moving distance L_n in a cycle depends on the cycle length s; that is, L_n is stochastically larger as s is larger. Hence, we provide the distribution of V_n, instead of L_n, and that of ψ_n for our mobility model and assume that these distributions do not depend on the cycle length. The distributions of V_n and ψ_n respectively represent changes in speed and direction of the typical UE over cycles of the skipping period, and the choice of these distributions gives enough flexibility to our model to capture various mobility patterns. For instance, $\mathbb{P}(V_n = 0) > 0$ represents that the UE can take a pause for s time slots with a positive probability, and if ψ_n takes a constant, the UE always moves along a straight line.

D. Performance Metrics

As discussed in Sec. I, the HO skipping induces the trade-off between the HO rate and the data rate. We thus evaluate the performance of our proposed scheme in terms of the expected downlink data rate $\mathcal{T}$ and the HO rate $\mathcal{H}$, which are respectively defined as

$$\mathcal{T} = \lim_{m\to\infty} \frac{1}{m}\mathbb{E}\left[\sum_{t=0}^{m-1} \xi(t)\right], \tag{6}$$

$$\mathcal{H} = \lim_{m\to\infty} \frac{\mathbb{E}[\zeta(0,m)]}{m}, \tag{7}$$

where $\xi(t)$ denotes the instantaneous downlink data rate for the typical UE at slot t, specifically given in (3), and $\zeta(a,b)$ denotes the number of HOs executed by the typical UE from slot a to slot b. These performance metrics are analyzed and evaluated in the following sections.

III. Performance Analysis and Evaluation

In this section, we investigate the performance of our proposed scheme introduced in the preceding section. For comparison, we analyze the performance metrics defined in (6) and (7) not only in the scenario with the proposed periodic HO skipping but also in the conventional scenario without any HO skipping on the same network and mobility models described in Secs. II-A and II-C. In the scenario without HO skipping, the typical UE certainly executes an HO whenever it crosses a boundary between two cells. We refer to the scenario without HO skipping and that with the periodic HO skipping as Scenario 0 and Scenario 1, respectively, and distinguish elements in the respective scenarios by putting the superscript "(0)" or "(1)"; for example, $\mathcal{T}^{(0)}$ and $\mathcal{H}^{(0)}$ respectively stand for the expected downlink data rate and the HO rate in Scenario 0, whereas $\mathcal{T}^{(1)}$ and $\mathcal{H}^{(1)}$ are those in Scenario 1.

A. Expected Downlink Data Rate Analysis

1) Expected Downlink Data Rate in Scenario 0: In Scenario 0, the typical UE certainly executes an HO whenever it crosses a boundary between two cells; that is, the typical UE is always connected to its nearest BS. The following proposition is directly derived from the existing result in the literature.

Proposition 1: For the cellular network model described in Sec. II, the expected downlink data rate in Scenario 0 is given by

$$\mathcal{T}^{(0)} = \int_0^\infty\int_0^\infty \frac{\rho(z,w)}{1+z}\,\mathrm{d}z\,\mathrm{d}w, \tag{8}$$

where

$$\rho(z,w) = \exp\biggl(-\sigma^2 z \left(\frac{w}{\pi\lambda}\right)^{\beta/2} - w\left(1 + \frac{2z^{2/\beta}}{\beta}\int_{1/z}^{\infty} \frac{v^{2/\beta-1}}{1+v}\,\mathrm{d}v\right)\biggr).$$

Proof: For $\boldsymbol{u} \in \mathbb{R}^2$, let $B(\boldsymbol{u})$ denote the index of the nearest point of $\Phi = \sum_{i\in\mathbb{N}} \delta_{X_i}$ to the location $\boldsymbol{u}$; that is, $\|X_{B(\boldsymbol{u})} - \boldsymbol{u}\| < \|X_i - \boldsymbol{u}\|$ for $i \in \mathbb{N} \setminus \{B(\boldsymbol{u})\}$. Suppose that the typical UE is located at $S(t) = \boldsymbol{u}$ at slot $t \in \mathbb{N}_0$. Since $\sum_{i=1}^{\infty} \delta_{X_i - \boldsymbol{u}}$ is equal in distribution to Φ due to the stationarity and $H_{i,t}$, $i \in \mathbb{N}$, $t \in \mathbb{N}_0$, are i.i.d., we have from (1) with (2) that $\mathsf{SINR}_{\boldsymbol{u},B(\boldsymbol{u})}(t)$ is equal in distribution to $\mathsf{SINR}_{\boldsymbol{0},B(\boldsymbol{0})}(0)$ for any $\boldsymbol{u} \in \mathbb{R}^2$. Thus, since $\{S(t)\}_{t\in\mathbb{N}_0}$ is independent of Φ and $\{H_{i,t}\}_{i\in\mathbb{N},t\in\mathbb{N}_0}$, the definition of the expected downlink data rate in (6) leads to

$$\begin{aligned}\mathcal{T}^{(0)} &= \lim_{m\to\infty} \frac{1}{m} \sum_{t=0}^{m-1} \mathbb{E}[\xi_{S(t),B(S(t))}(t)] \\ &= \mathbb{E}[\xi_{\boldsymbol{0},B(\boldsymbol{0})}(0)],\end{aligned}$$

which implies that the expected downlink data rate in Scenario 0 is equal to that for a static UE. Hence, the existing result of the expected downlink data rate for a static UE gives (8) (see, e.g., [21, Theorem 3]). ■

Remark 1: Proposition 1 implies that, if a moving UE is always connected to its nearest BS, the expected downlink data rate is identical to that for a static UE. Note that this fact is derived under the condition that Φ is stationary, $H_{i,t}$, $i \in \mathbb{N}$, $t \in \mathbb{N}_0$, are i.i.d., and $\{S(t)\}_{t\in\mathbb{N}_0}$ is independent of Φ and $\{H_{i,t}\}_{i\in\mathbb{N},t\in\mathbb{N}_0}$. In other words, this holds true even when the locations of BSs are according to a general stationary point process and the fading effects independently follow a general identical distribution. A similar discussion is found in [20, Remark 2].

2) Expected Downlink Data Rate in Scenario 1: In Scenario 1, the typical UE is not always connected to its nearest BS but remains connected to the BS that is the nearest at the beginning of each cycle of the skipping period.

Theorem 1: For the cellular network model described in Sec. II, the expected downlink data rate in Scenario 1 with s slots of the skipping period is given by

$$\mathcal{T}^{(1)} = \frac{1}{s}\sum_{t=0}^{s-1} \int_0^{\infty} \tau(tv)\,\mathrm{d}F_V(v), \tag{9}$$

where F_V denotes the distribution function of the moving speed $V_1 = \|Y_1\|/s$ of the typical UE in a cycle of s slots and

$$\tau(u) = \int_0^{\infty} \frac{1}{z}\,\exp\bigl(-\sigma^2 z - \pi\lambda\, K_\beta\, z^{2/\beta}\bigr)\,\bigl(\mu(z,u) - 1\bigr)\,\mathrm{d}z, \tag{10}$$

with

$$K_\beta = \frac{2\pi}{\beta}\,\csc\frac{2\pi}{\beta}, \tag{11}$$

$$\mu(z,u) = 2\pi\lambda\int_0^\infty r\exp\bigl(-\lambda\left[\pi r^2 - J(r,z,u)\right]\bigr)\,\mathrm{d}r, \tag{12}$$

$$J(r,z,u) = 2z\int_0^\pi\!\!\int_0^r \frac{x}{z + w_{x,u,\phi}{}^\beta}\,\mathrm{d}x\,\mathrm{d}\phi, \tag{13}$$

and $w_{x,u,\phi} = \sqrt{x^2 + u^2 - 2xu\cos\phi}$.

The proof of Theorem 1 relies on the following lemma.

Lemma 1: Suppose that a UE is located at $\boldsymbol{u} \in \mathbb{R}^2$ with $\|\boldsymbol{u}\| = u$ at slot $t \in \{0,1,\dots,s-1\}$ and is served by the BS at $X_{B(\mathbf{0})}$, which is the nearest BS to the origin. Then, the expected instantaneous downlink data rate for this UE satisfies $\mathbb{E}[\xi_{\boldsymbol{u},B(\mathbf{0})}(t)] = \tau(u)$ given in (10).

Proof: See Appendix A ■

Proof of Theorem 1: As in the proof of Proposition 1, let $B(\boldsymbol{u})$ denote the index of the nearest point of $\Phi = \sum_{i\in\mathbb{N}}\delta_{X_i}$ to $\boldsymbol{u} \in \mathbb{R}^2$. In Scenario 1, we see from (4) and (5) that the typical UE is connected to the BS at $X_{B(S(ns))}$ at slot $ns+t$ for $n \in \mathbb{N}_0$ and $t \in \{0,1,\dots,s-1\}$. Thus, the expected downlink data rate in (6) is reduced to

$$\begin{aligned}\mathcal{T}^{(1)} &= \lim_{m\to\infty}\frac{1}{m}\sum_{n=0}^{\lfloor m/s\rfloor}\sum_{t=0}^{s-1}\mathbb{E}\bigl[\xi_{S(ns+t),B(S(ns))}(ns+t)\bigr] \\ &= \frac{1}{s}\sum_{t=0}^{s-1}\mathbb{E}[\xi_{S(t),B(\mathbf{0})}(t)],\end{aligned} \tag{14}$$

where the last equality follows from the distributional equivalence of $\mathsf{SINR}_{S(ns+t),B(S(ns))}(ns+t)$ and $\mathsf{SINR}_{S(t),B(\mathbf{0})}(t)$ for $t \in \{0,1,\dots,s-1\}$, which follows because Φ is stationary and isotropic, $H_{i,t}$, $i \in \mathbb{N}$, $t \in \mathbb{N}_0$, are i.i.d., and also Y_k, $k \in \mathbb{N}$, in (4) are i.i.d. and independent of Φ and $\{H_{i,t}\}_{i\in\mathbb{N},t\in\mathbb{N}_0}$. Hence, we obtain (9) since $\mathbb{E}[\xi_{S(t),B(\mathbf{0})}(t) \mid S(t) = \boldsymbol{u}] = \tau(tv)$ when $\|\boldsymbol{u}\| = tv$ by Lemma 1 and $\|S(t)\| = (t/s)\,\|Y_1\| = tV_1$ for $t \in \{0,1,\dots,s-1\}$ by (5). ■

The expressions (9)–(13) obtained in Theorem 1 are indeed numerically computable. However, they include some nested integrals, which may annoy us with a heavy computational load. In the rest of this subsection, we discuss some ways of reducing the computational load.

3) Tips for Computational Load Reduction: We here introduce some tips to reduce the load of computing $\mathcal{T}^{(1)}$ in Theorem 1 exactly or approximately. First, we find that a simple change of variables reduces the number of nested integrals.

TABLE I

COMPARISON OF THE COMPUTATION TIME OF $\tau(u)$ USING (13) AND (15). THE PARAMETER VALUES ARE FIXED AT $\lambda = 10$ (units/km^2), $\beta = 3$ AND $\sigma^2 = 25$.

u (km)	0.1	0.2	0.3	0.4	0.5	0.6
Use of eq. (13) (sec)	1344	973	10221	7286	4754	1474
Use of eq. (15) (sec)	695	1118	1196	632	974	401

Lemma 2: Function J in (13) is equal to the following.

$$J(r,z,u) = 2z \int_0^{u+r} \frac{x}{z + x^\beta}\, C(x,r,u)\, \mathrm{d}x, \tag{15}$$

with

$$C(x,r,u) = \begin{cases} \pi, & u = 0, \\ \arccos\left(-1 \vee \dfrac{x^2+u^2-r^2}{2xu} \wedge 1\right), & u > 0, \end{cases}$$

where $a \vee b = \max\{a,b\}$ and $a \wedge b = \min\{a,b\}$ for $a, b \in \mathbb{R}$.

Proof: See Appendix B ■

We can observe through experiments that (15) reduces the computation time of the expected instantaneous downlink data rate $\tau(u)$ by about 60% on average compared to the use of (13) (see Table I). Next, we give a simple lower bound for τ in (10) under the interference-limited (noise-free) assumption.

Corollary 1: Suppose that $\sigma^2 = 0$. Then, τ in (10) is bounded below as follows.

$$\tau(u) \ge \frac{\beta}{2} \int_0^\infty \frac{z^{\beta/2-1}}{(1+z)({K_\beta}^{\beta/2} + z^{\beta/2})} \exp\left(-\pi\lambda\, u^2\, \frac{z}{1+z}\right) \mathrm{d}z, \quad u \ge 0, \tag{16}$$

with K_β given in (11).

Proof: See Appendix C. ■

Remark 2: As we can see in the proof, the lower bound in Corollary 1 is obtained by relaxing the condition that there must not be other BSs closer than the nearest BS to the origin. Similar bounds/approximates are often found in the literature (see, e.g., [25]).

The lower bound obtained in Corollary 1 is indeed of a simple form (including a single integral), but as seen in Fig. 2, it causes non-negligible gaps from the exact values, in particular when the moving distance u is small, whereas the gaps decrease as u increases. On the other hand, we know that $\tau(0) = \mathcal{T}^{(0)}$ since the expected downlink data rate in Scenario 0 is equal to that for a static UE. Hence, we can approximate τ in (10) by interpolating between $\mathcal{T}^{(0)}$ and

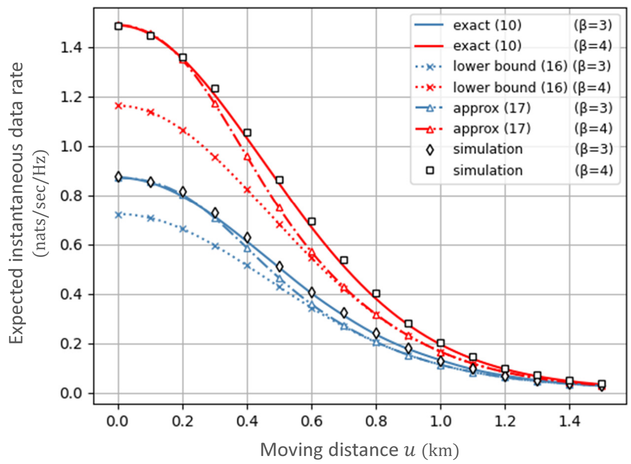

Fig. 2. Numerical comparison of τ in (10) with the lower bound (16), the approximation (17), and the values from Monte Carlo simulation. The BS intensity is fixed at $\lambda = 1$ (units/km^2) and two patterns of $\beta = 3$ and $\beta = 4$ are exhibited.

the lower bound in Corollary 1 as follows. Suppose $\sigma^2 = 0$ as in Corollary 1 and let $\widetilde{\tau}$ denote the lower bound of τ given on the right-hand side of (16). Then, τ in (10) is approximated as

$$\tau(u) \approx \epsilon(u)\,\mathcal{T}^{(0)} + (1 - \epsilon(u))\,\widetilde{\tau}(u), \quad u \ge 0, \tag{17}$$

where a function ϵ: $[0, \infty) \to [0, 1]$ is smooth and decreasing, and satisfies $\epsilon(0) = 1$ and $\epsilon(u) \to 0$ as $u \to \infty$; that is, it is chosen in such a way that the right-hand side of (17) is close to $\mathcal{T}^{(0)}$ when u is small, and it approaches $\widetilde{\tau}(u)$ as u becomes larger. Figure 2 compares the numerical results of τ in (10) with its lower bound in (16) and the approximation in (17), as well as with the values from Monte Carlo simulation, with respect to the moving distance u. In the approximation (17), the function ϵ is set as $\epsilon(u) = e^{-10\,u^2}$, $u \ge 0$. The simulation results are computed as the mean of 10,000 independent samples. As stated above, the values of the lower bound have some gaps from the exact values when u is small, whereas these gaps decrease as u increases. This implies that the condition that other BSs never exist closer than the nearest BS is nonnegligible when the typical UE is close to the origin, but it is diminishing as the UE moves away from the origin. On the other hand, the approximation (17) shows good agreement with the exact values as expected. However, we should note that such agreement depends on a choice of the function ϵ. An exponential function $\epsilon(u) = e^{-au^b}$ as above seems an plausible choice as one with the desired properties (that is, smooth and decreasing with $\epsilon(0) = 1$ and $\lim_{u\to\infty} \epsilon(u) = 0$), and statistical fitting of a and b would lead to better results.

B. Handover Rate Analysis

We now proceed to the analysis of the HO rate. Similar to the proof of Theorem 1, the HO rate in (7) is reduced to

$$\begin{aligned}\mathcal{H} &= \lim_{m\to\infty}\frac{1}{m}\sum_{n=0}^{\lfloor m/s\rfloor}\mathbb{E}[\zeta(ns,(n+1)s)]\\ &= \frac{\mathbb{E}[\zeta(0,s)]}{s},\end{aligned}\tag{18}$$

where the last equality follows since Φ is stationary and isotropic, and Y_k, $k\in\mathbb{N}$, in (4) are i.i.d. and independent of Φ. By (18), it is enough to consider the expected number of HOs in a cycle of s slots, during which the typical UE moves along a straight line segment, and we can use the existing results in both Scenarios 0 and 1.

1) HO Rate in Scenario 0: The HO rate in the scenario without any HO skipping has so far been studied in the literature. The following is a direct consequence of it.

Proposition 2: For the cellular network model described in Sec. II, the HO rate in Scenario 0 is given by

$$\mathcal{H}^{(0)} = \frac{4\sqrt{\lambda}\,\overline{v}}{\pi},\tag{19}$$

where $\overline{v}$ denotes the average moving speed of the typical UE in a cycle of s slots; that is, $\overline{v}=\mathbb{E}[V_1]$ with $V_1 = \|Y_1\|/s$.

Proof: Given $L_1=\|Y_1\|=\ell$, the conditionally expected number of HOs $\mathbb{E}[\zeta^{(0)}(0,s)\mid L_1=\ell]$ in a cycle is equal to the expected number of intersections of a line segment of length ℓ with the boundaries of the Poisson-Voronoi cells, and is well-known as $\mathbb{E}[\zeta^{(0)}(0,s)\mid L_1=\ell]=4\sqrt{\lambda}\,\ell/\pi$ (see, e.g., [15], [26], [27]). Applying this to (18) with $L_1 = sV_1$ derives (19) by taking the expectation. ■

2) HO Rate in Scenario 1: The HO rate in a similar scenario to our Scenario 1 is studied in [19], which helps us to show the following.

Proposition 3: For the cellular network model described in Sec. II, the HO rate in Scenario 1 with s slots of the skipping period is given by

$$\mathcal{H}^{(1)} = \frac{1}{s}\left[1-2\lambda\int_0^\infty\!\!\int_0^\pi\!\!\int_0^\infty r\,e^{-\lambda\,\eta(r,sv,\phi)}\,\mathrm{d}r\,\mathrm{d}\phi\,\mathrm{d}F_V(v)\right],\tag{20}$$

where

$$\eta(r,\ell,\phi) = {w_{r,\ell,\phi}}^2\,\arccos\!\left(\frac{r\cos\phi-\ell}{w_{r,\ell,\phi}}\right)+r^2(\pi-\phi)+r\ell\sin\phi,\tag{21}$$

with $w_{r,\ell,\phi} = \sqrt{r^2 + \ell^2 - 2r\ell\cos\phi}$, and F_V is (as in (9)) the distribution function of the moving speed $V_1 = \|Y_1\|/s$ of the typical UE in a cycle of s slots.

Proof: By the isotropy of $\Phi = \sum_{i\in\mathbb{N}} \delta_{X_i}$, we can assume without loss of generality that the typical UE moves in the positive direction along the horizontal axis during a cycle of s slots. Suppose that the typical UE initially connected to the BS at $X_{B(\mathbf{0})} = \boldsymbol{x} = (r, \phi)$ in the polar coordinates and moves to $Y_1 = \boldsymbol{y} = (\ell, 0)$ in s slots. Let $b_{\boldsymbol{x}}(r)$ denote the disk centered at $\boldsymbol{x} \in \mathbb{R}^2$ with radius $r > 0$. Since there are no BSs in $b_{\mathbf{0}}(r)$ and the distance to the initial BS at $\boldsymbol{x}$ from the location $\boldsymbol{y}$ is equal to $w_{r,\ell,\phi} = \sqrt{r^2 + \ell^2 - 2r\ell\cos\phi}$, the typical UE executes an HO at the end of the cycle if and only if there is at least one BS in the area $b_{\boldsymbol{y}}(w_{r,\ell,\phi}) \setminus b_{\mathbf{0}}(r)$. Hence, similar discussion to [19] gives

$$\begin{aligned}
&\mathbb{E}\big[\zeta^{(1)}(0, s) \mid X_{B(\mathbf{0})} = (r, \phi), Y_1 = (\ell, 0)\big] \\
&= 1 - e^{-\lambda\,|b_{\boldsymbol{y}}(w_{r,\ell,\phi})\setminus b_{\mathbf{0}}(r)|} \\
&= 1 - \exp\!\left(-\lambda\left[{w_{r,\ell,\phi}}^2 \arccos\!\left(\frac{r\cos\phi - \ell}{w_{r,\ell,\phi}}\right) - r^2\phi + r\ell\sin\phi\right]\right),
\end{aligned} \tag{22}$$

where $|A|$ denotes the Lebesgue measure of $A \in \mathcal{B}(\mathbb{R}^2)$. This can be unconditioned by integrating with respect to the density $f_0(r)\,\mathrm{d}r = 2\pi\lambda r\, e^{-\pi\lambda r^2}\,\mathrm{d}r$ of $\|X_{B(\mathbf{0})}\|$ over $[0, \infty)$, $\mathrm{d}\phi/\pi$ over $[0, \pi)$, and $\mathrm{d}F_V(v)$ over $[0, \infty)$ with $v = \ell/s$. Finally, plugging it into (18), we have (20). ■

C. Numerical Evaluation of Performance Metrics

We here numerically evaluate the expected downlink data rate and the HO rate in the periodic HO skipping scheme, which are respectively obtained in Theorem 1 (with Lemma 2) and Proposition 3. Throughout the experiments, we set as 1slot = 1msec, the intensity of the BSs, the path-loss exponent, and the noise power are fixed at $\lambda = 10$ (units/km^2), $\beta = 3$, and $\sigma^2 = 25$, respectively, and the moving speed $V_1 = \|L_1\|/s$ of the typical UE is given as a constant. Figure 3 shows the curves of $\mathcal{T}^{(1)}$ and $\mathcal{H}^{(1)}$ with respect to the length s of the skipping period. For comparison, the values from Monte Carlo simulation are also plotted as the means of 1,000 independent samples of $\sum_{t=0}^{m-1} \xi^{(1)}(t)/m$ and $\zeta^{(1)}(0, m)/m$, respectively with $m = 1000$ (cf. (6) and (7)). We find that the analytical results match well with the simulation results. Moreover, we can confirm the trade-off relation between the HO rate and the expected downlink data rate; that is, both are decreasing in the length of the skipping period. We further explore this trade-off in the next subsection.

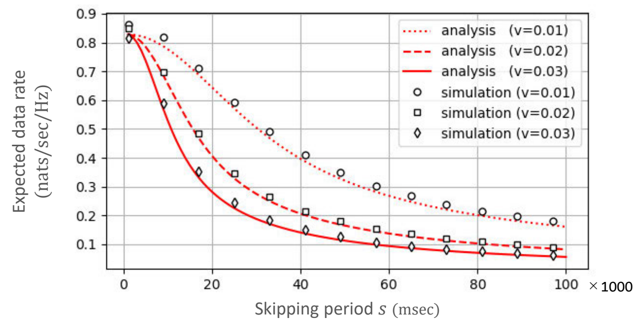

(a) The expected downlink data rate.

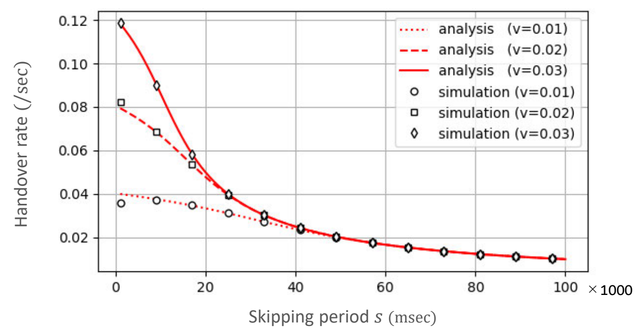

(b) The HO rate.

Fig. 3. The performance metrics as functions of the length s of the skipping period for three patterns of the moving speed $v = 0.01$, 0.02, and 0.03 (km/sec).

D. Utility Metric

To discuss the trade-off between the expected downlink data rate $\mathcal{T}$ and the HO rate $\mathcal{H}$, we introduce a utility metric $\mathcal{U}$ as

$$\mathcal{U} = \mathcal{T} - c\,\mathcal{H}, \tag{23}$$

where a utility constant $c > 0$ is suitably chosen so as to convert the negative impact of HOs into the loss of the downlink data rate. Note that similar metrics are found in the literature (cf. [5], [12], [17], [18]) and are often referred to as the user throughput accounting for the loss due to HOs. However, we do not use the term "throughput" in this paper because $\mathcal{U}$ in (23) can take negative values (see, e.g., Figs. 4 and 5 below).

Figure 4 compares the utility metrics $\mathcal{U}^{(0)}$ and $\mathcal{U}^{(1)}$ respectively for Scenarios 0 and 1 with respect to the average speed $\overline{v} = \mathbb{E}[V_1]$ of the typical UE. In the computation of $\mathcal{U}^{(1)}$, τ in (9) is replaced by its approximation (17) with the adjustment function $\epsilon(u) = e^{-10\,u^2}$. Four different distributions of the moving speed are experimented with the common average $\overline{v}$; that is, exponential, second-order Erlang, second-order hyper-exponential, and deterministic ones,

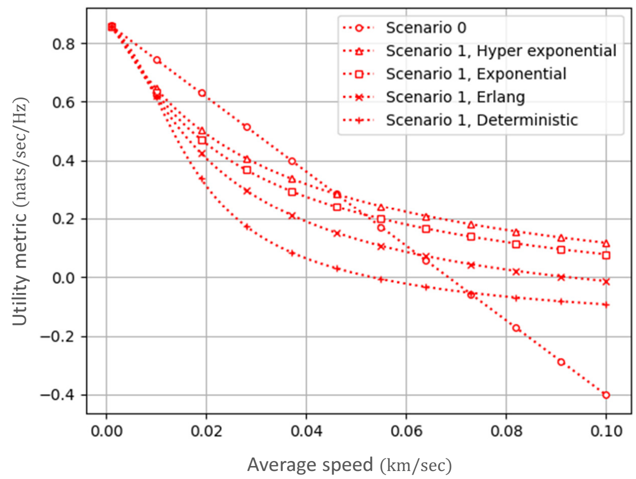

Fig. 4. The values of $\mathcal{U}^{(0)}$ and $\mathcal{U}^{(1)}$ as functions of the average speed $\overline{v}$ of the moving UE with several distributions.

where in the hyper-exponential distribution, two exponential distributions with means $\overline{v}/2$ and $3\overline{v}/2$ are mixed with equal probability. The other parameters are fixed as $\lambda = 1$ (units/km^2), $\beta = 3$, $\sigma^2 = 0$, $s = 50,000$ (msec), and $c = 10$ (nats/Hz). Note that only one line is exhibited for $\mathcal{U}^{(0)}$ since it depends on the distribution of the moving speed only through its average (as confirmed from (8) and (19)). From Fig. 4, we observe that Scenario 0 shows better performance when the average moving speed is small (roughly $\overline{v} \le 0.05$ (km/sec)), whereas Scenario 1 becomes better as the UE moves faster. This is thought to be because $\mathcal{H}^{(0)}$ is linearly increasing in $\overline{v}$ (see (19)), whereas $\tau(u)$ in (10) is slowly decreasing in u (see Fig. 2). Moreover, we find an interesting property from the experiment that the distribution of the moving speed has an impact on the utility metric in Scenario 1; that is, the utility metric takes larger values as the distribution of the moving speed is larger in variation. Exploration of this property will be left for future work.

IV. Optimal Skipping Period

As stated in Sec. II-B, the choice of the length of the skipping period is vital for our proposed scheme. In this section, we discuss how to decide the length s of the skipping period on the basis of the analysis in the preceding section. We here consider only Scenario 1—the periodic HO skipping scenario—so that we omit the superscript "(1)" and just write $\mathcal{T}$, $\mathcal{H}$ and $\mathcal{U}$.

A. Approximate Derivation of Optimal Skipping Period

Let us see Fig. 5, where the numerical results of the utility metric $\mathcal{U}$ in (23) and its lower bound, obtained by replacing τ in (9) with the right-hand side of (16), are plotted as functions

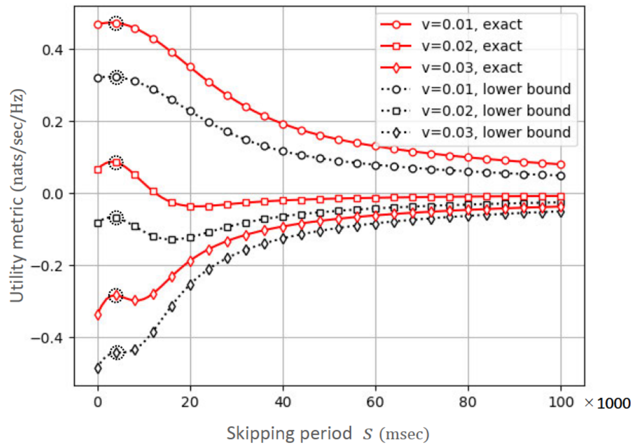

Fig. 5. The values of utility metric and its lower bound as functions of the skipping period s.

of the length s of the skipping period (in 1slot = 1msec) for three different values of constant moving speed of the typical UE. In this experiment, the parameters are set as $\lambda = 10$ (units/km^2), $\beta = 3$, $\sigma^2 = 0$, and $c = 10$ (nats/Hz). From the figure, we find that the utility metric has a local maximum (at around $s = 4,000$ (msec)) and this local maximum looks global when the moving speed is small. We refer to the length s of the skipping period which gives the local maximum of the utility metric as the *optimal skipping period*. Furthermore, we should notice that the values of the optimal skipping period are almost the same as those locally maximizing the lower bound of $\mathcal{U}$ and are hardly affected by the difference in the moving speed. This suggests that we can approximately obtain the optimal skipping period by finding the length s which locally maximizes the lower bound of $\mathcal{U}$ for a certain moving speed of the typical UE. From this observation, we have the following.

Theorem 2: For the cellular network model described in Sec. II, we suppose that the typical UE adopts the periodic HO skipping and moves at certain constant speed. Then, an approximation of the optimal skipping period is obtained as the closest integer of s^* given by

$$s^* = \left(\frac{15}{\pi^2} - 1\right)\frac{c}{2\beta}\left(\int_0^\infty \frac{z^{\beta/2}}{(1+z)^2({K_\beta}^{\beta/2} + z^{\beta/2})}\,\mathrm{d}z\right)^{-1}, \tag{24}$$

where K_β is given in (11).

Proof: The proof approximately derives the length s of the skipping period which maximizes the lower bound of the utility metric for sufficiently small moving speed of the typical UE. The details are given in Appendix D. ∎

Remark 3: Theorem 2 is shown under the condition that the moving speed v of the typical UE is sufficiently small (so that the terms of $o(v^2)$ are negligible). Indeed, as seen in Fig. 5, the optimal skipping period is hardly affected by the difference in the moving speed within the range of the experiment. A further advantage of s^* in (24) is that it is determined only by the path-loss exponent β and the utility constant c introduced in (23), but does not depend on the BS intensity as well as the moving speed. In other words, we can use s^* in (24) regardless of the moving speed and the BS intensity. Some properties of s^* are revealed through numerical experiments in the next subsection.

B. Numerical Evaluation of s^*

We here numerically evaluate s^* obtained in Theorem 2. Figure 6 shows the numerical results of s^* (in 1slot = 1msec) with respect to the path-loss exponent β and the utility constant c. The BS intensity and the moving speed of the typical UE are fixed as $\lambda = 1$ (units/km^2) and $v = 0.01$ (km/sec), respectively. For comparison, the values of s, which locally maximize the lower bound of the utility metric, obtained by replacing τ in (9) with its lower bound given in (16), are numerically searched and plotted in the figure. From Fig. 6, we observe that the values of s^* agree well with the values from the numerical search even for positive moving speed, in particular for large β and small c, in spite that s^* is derived under the condition of sufficiently small moving speed. Figure 6a shows that s^* is decreasing in β. This is thought to be because $\tau(u)$ decays more rapidly with respect to u when β is larger (as confirmed in Fig. 2); that is, smaller s brings better performance when β is larger since $\mathcal{T}(s) = \sum_{t=0}^{s-1} \tau(tv)/s$. On the other hand, Fig. 6b shows that s^* is linearly increasing in c (as is clear from (24)). This is interpreted as because the utility metric in (23) is linearly decreasing in c, and thus better performance is given by larger s which makes the HO rate lower.

Figure 7 further compares the values of s^* in (24) and the numerically searched values of s as above with respect to the constant moving speed v of the typical UE. Since s^* does not depend on v and λ (see (24)), its value is given as a horizontal line for each pair of β and c. Note that the values of the optimal skipping period obtained by the numerical search do not change significantly with respect to the changes in v and λ, in particular for large β and small c, which allows us to use s^* in (24) as an approximation of the optimal skipping period for any v and λ, in particular when β is large and c is small.

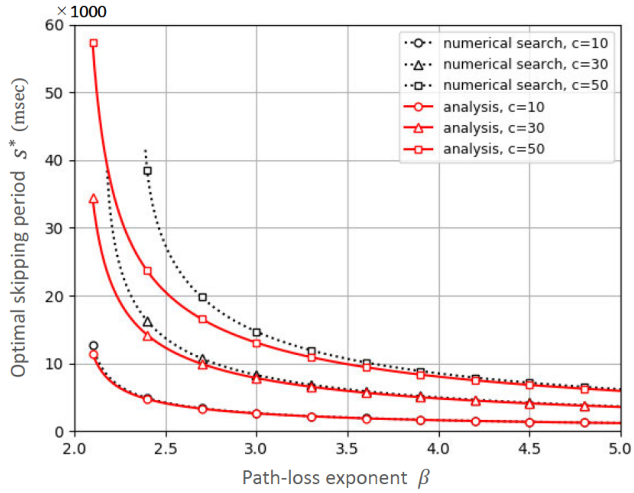

(a) s^* as a function of β.

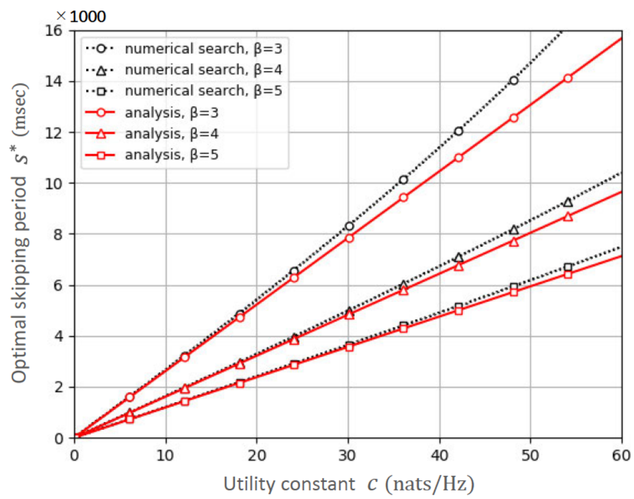

(b) s^* as a function of c.

Fig. 6. The values of s^* in (24) with respect to the path-loss exponent β and the utility constant c in (23).

V. Comparison with Other Techniques

We now compare our proposed scheme with two other related HO skipping techniques—the alternate HO skipping in [4] and the topology-aware HO skipping in [8]. We use the utility metric $\mathcal{U}$ in (23) for the comparison study. In the computation of $\mathcal{U}$ in our proposed scheme, we adopt the approximate optimal skipping period obtained in Theorem 2, and in the computation of the expected downlink data rate, τ in (9) is replaced by its approximation (17) with the adjustment function $\epsilon(u) = e^{-10u^2}$, $u \geq 0$. In the other two comparison techniques, the expected downlink data rates and the HO rates are computed using Monte Carlo simulation. The numerical results are shown in Fig. 8, where we set as 1slot = 1msec and the values of the utility metrics

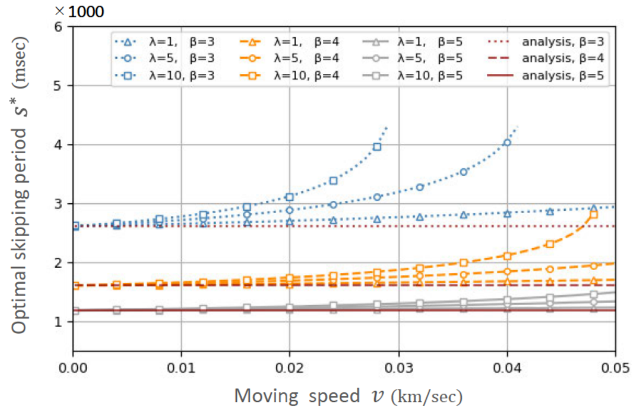

(a) s^* as a function of v with several patterns of λ and β, where $c = 10$ (nats/Hz) is fixed.

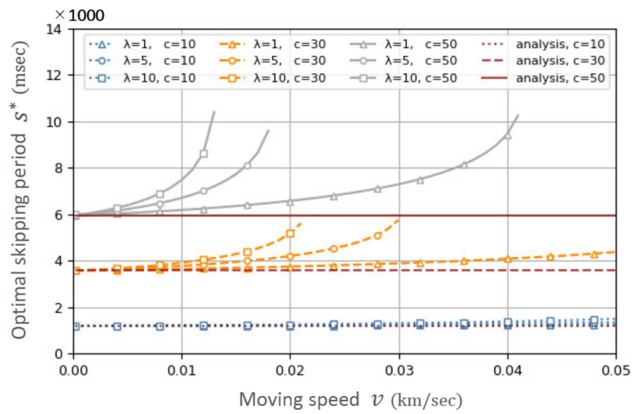

(b) s^* as a function of v with several patterns of λ and c, where $\beta = 5$ is fixed.

Fig. 7. The values of s^* in (24) with respect to the moving speed v of the typical UE.

with respect to the BS intensity λ are plotted. In the topology-aware HO skipping, the chord length threshold is fixed as $M = 0.3$ (km) (see [8] for details). The other parameters are set as $\beta = 3$, $c = 10$ (nats/Hz), and the moving speed is constant as $v = 0.01$ (km/sec). From the figure, we observe that our proposed scheme can outperform the other two techniques depending on the parameter setting. Although it is not possible to examine all the combinations of parameter setting, we could at least assert that our proposed scheme is comparable to the other sophisticated techniques in spite of its simpleness.

VI. Conclusion

In this paper, we have proposed a simple HO skipping scheme in cellular networks, called the periodic HO skipping, and have evaluated its performance analytically and numerically.

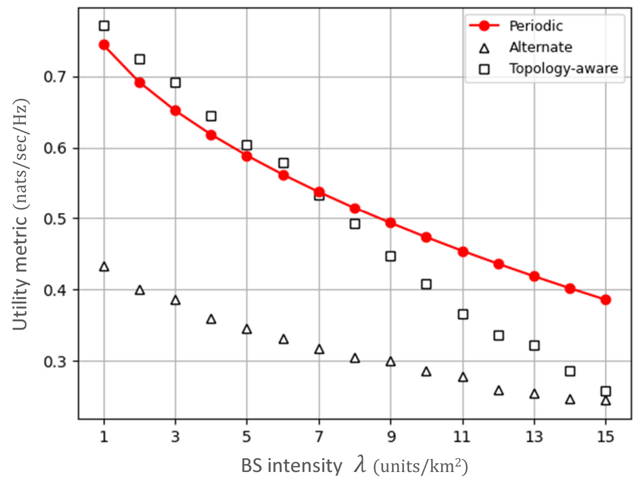

Fig. 8. Numerical comparison of the utility metrics for the periodic HO skipping and other related HO skipping techniques.

Specifically, applying the stochastic geometry approach, we have derived numerically computable expressions for the expected downlink data rate and the HO rate when the UE adopts the proposed scheme. Through the numerical experiments based on the analysis, we have confirmed that the proposed scheme can outperform the scenario without any HO skipping in terms of a utility metric representing the trade-off between the expected downlink data rate and the HO rate, in particular when the UE moves fast. Moreover, we have discussed how to decide the length of the skipping period and have provided a simple computable expression of the skipping period which approximately gives a local maximum of the utility metric. Numerical comparison with other related HO skipping techniques have also shown that the proposed scheme is comparable to the others. Although we have considered here a simple mobility model on a homogeneous PPP network model, further development within more extended and generalized frameworks (e.g., HetNets with interference cancellation and/or the BS cooperation) would be expected for future work and one direction of the extensions is found in [28].

Appendix A
Proof of Lemma 1

Applying Hamdi's Lemma [29, Lemma 1] to the expectation of (3) with (1), (2) and $i = B(\mathbf{0})$, we have

$$\mathbb{E}[\xi_{\boldsymbol{u},B(\mathbf{0})}(t)] = \mathbb{E}\left[\log\left(1 + \frac{H_{B(\mathbf{0}),t}\,\|X_{B(\mathbf{0})} - \boldsymbol{u}\|^{-\beta}}{I_{\boldsymbol{u},B(\mathbf{0})}(t) + \sigma^2}\right)\right]$$

$$= \int_0^\infty \frac{e^{-\sigma^2 z}}{z} \left(\mathbb{E}\left[e^{-z\, I_{\boldsymbol{u},B(\boldsymbol{0})}(t)} \right] - \mathbb{E}\left[e^{-z \sum_{j\in\mathbb{N}} H_{j,t}\, \|X_j - \boldsymbol{u}\|^{-\beta}} \right] \right) \mathrm{d}z. \tag{25}$$

For the second expectation in the last expression above, the Laplace transform of an exponential distribution and the generating functional of a PPP (e.g., [30, Example 9.4(c)]) yield

$$\begin{aligned} \mathbb{E}\left[\prod_{j\in\mathbb{N}} e^{-z\, H_{j,t}\, \|X_j - \boldsymbol{u}\|^{-\beta}} \right] &= \mathbb{E}\left[\prod_{j\in\mathbb{N}} \left(1 + \frac{z}{\|X_j - \boldsymbol{u}\|^\beta} \right)^{-1} \right] \\ &= \exp\left(-\lambda\, z \int_{\mathbb{R}^2} \frac{1}{z + \|\boldsymbol{x}\|^\beta}\, \mathrm{d}\boldsymbol{x} \right) \\ &= e^{-\pi\lambda K_\beta\, z^{2/\beta}}, \end{aligned} \tag{26}$$

with $K_\beta = (2\pi/\beta)\csc(2\pi/\beta)$ as given in (11), where we use the polar coordinate conversion and $\int_0^\infty w^{a-1}/(1+w)\,\mathrm{d}w = \pi \csc a\pi$ for $a \in (0,1)$ in the last equality. Next, we consider the first expectation in the last expression of (25), which satisfies

$$\mathbb{E}\left[e^{-z\, I_{\boldsymbol{u},B(\boldsymbol{0})}(t)} \right] = \int_0^\infty \mathbb{E}\left[e^{-z\, I_{\boldsymbol{u},B(\boldsymbol{0})}(t)} \;\middle|\; \|X_{B(\boldsymbol{0})}\| = r \right] f_0(r)\, \mathrm{d}r, \tag{27}$$

where $f_0(r) = 2\pi\lambda\, r e^{-\pi\lambda r^2}$ gives the probability density function of $\|X_{B(\boldsymbol{0})}\|$. Similar to obtaining (26), we have

$$\begin{aligned} &\mathbb{E}\left[e^{-z\, I_{\boldsymbol{u},B(\boldsymbol{0})}(t)} \;\middle|\; \|X_{B(\boldsymbol{0})}\| = r \right] \\ &= \mathbb{E}\left[\prod_{j\in\mathbb{N}\setminus\{B(\boldsymbol{0})\}} \left(1 + \frac{z}{\|X_j - \boldsymbol{u}\|^\beta} \right)^{-1} \;\middle|\; \|X_{B(\boldsymbol{0})}\| = r \right] \\ &= \exp\left(-\lambda\, z \int_{\|\boldsymbol{x}\|>r} \frac{1}{z + \|\boldsymbol{x} - \boldsymbol{u}\|^\beta}\, \mathrm{d}\boldsymbol{x} \right) \\ &= \exp\left(-\pi\lambda K_\beta\, z^{2/\beta} + \lambda\, z \int_{\|\boldsymbol{x}\|\le r} \frac{1}{z + \|\boldsymbol{x} - \boldsymbol{u}\|^\beta}\, \mathrm{d}\boldsymbol{x} \right), \end{aligned} \tag{28}$$

where the polar coordinate conversion gives

$$z \int_{\|\boldsymbol{x}\|\le r} \frac{1}{z + \|\boldsymbol{x} - \boldsymbol{u}\|^\beta}\, \mathrm{d}\boldsymbol{x} = J(r, z, u), \tag{29}$$

with J given in (13). Plugging (28) together with (29) into (27), we have

$$\mathbb{E}\left[e^{-z\, I_{\boldsymbol{u},B(\boldsymbol{0})}(t)} \right] = e^{-\pi\lambda K_\beta\, z^{2/\beta}}\, \mu(z, u), \tag{30}$$

with μ in (12). Finally, plugging (26) and (30) into (25) derives (10).

Appendix B
Proof of Lemma 2

It is immediate for the case of $u = 0$ since $w_{x,0,\phi} = x$ in (13). Suppose $u > 0$. On the left-hand side of (29), changing the variables as $\boldsymbol{x}' = \boldsymbol{u} - \boldsymbol{x}$ leads to

$$\int_{\|\boldsymbol{x}\|\le r} \frac{1}{z + \|\boldsymbol{x} - \boldsymbol{u}\|^\beta}\,\mathrm{d}\boldsymbol{x} = \int_{b_{\boldsymbol{u}}(r)} \frac{1}{z + \|\boldsymbol{x}'\|^\beta}\,\mathrm{d}\boldsymbol{x}',$$

where $b_{\boldsymbol{u}}(r)$ denotes the disk centered at $\boldsymbol{u} \in \mathbb{R}^2$ with radius $r > 0$. Recall that $\|\boldsymbol{u}\| = u$ as in Lemma 1. When $u \ge r$, the polar coordinate conversion gives (see Fig. 9a)

$$\begin{aligned}
&\int_{b_{\boldsymbol{u}}(r)} \frac{1}{z + \|\boldsymbol{x}\|^\beta}\,\mathrm{d}\boldsymbol{x} \\
&= 2\int_{u-r}^{u+r} \frac{x}{z + x^\beta}\,\arccos\Bigl(\frac{x^2 + u^2 - r^2}{2xu}\Bigr)\,\mathrm{d}x \\
&= 2\int_{0}^{u+r} \frac{x}{z + x^\beta}\,\arccos\Bigl(\frac{x^2 + u^2 - r^2}{2xu} \wedge 1\Bigr)\,\mathrm{d}x, \qquad (31)
\end{aligned}$$

where the last equality holds since $f(x) = (x^2 + u^2 - r^2)/(2xu) > 1$ for $x \in (0, u - r)$ with $f(u - r) = 1$ when $u \ge r > 0$. On the other hand, when $u < r$, we have similarly (see Fig. 9b),

$$\begin{aligned}
&\int_{b_{\boldsymbol{u}}(r)} \frac{1}{z + \|\boldsymbol{x}\|^\beta}\,\mathrm{d}\boldsymbol{x} \\
&= 2\pi\int_{0}^{r-u} \frac{x}{z + x^\beta}\,\mathrm{d}x + 2\int_{r-u}^{u+r} \frac{x}{z + x^\beta}\,\arccos\Bigl(\frac{x^2 + u^2 - r^2}{2xu}\Bigr)\,\mathrm{d}x \\
&= 2\int_{0}^{u+r} \frac{x}{z + x^\beta}\,\arccos\Bigl(-1 \vee \frac{x^2 + u^2 - r^2}{2xu}\Bigr)\,\mathrm{d}x, \qquad (32)
\end{aligned}$$

where the last equality holds since $f(x) = (x^2 + u^2 - r^2)/(2xu) < -1$ for $x \in (0, r - u)$ with $f(r - u) = -1$ when $0 < u < r$. Hence, unifying (31) and (32), we have (15) since $(x^2 + u^2 - r^2)/(2xu) \in [-1, 1]$ when $|u - r| \le x \le u + r$.

Appendix C
Proof of Corollary 1

In (25) with $\sigma^2 = 0$, changing the variables as $z' = \|X_{B(\mathbf{0})} - \boldsymbol{u}\|^{-\beta} z$ leads to

$$\begin{aligned}
&\mathbb{E}[\xi_{\boldsymbol{u},B(\mathbf{0})}(t)] \\
&= \int_0^\infty \frac{1}{z'}\,\mathbb{E}\Bigl[e^{-\|X_{B(\mathbf{0})}-\boldsymbol{u}\|^\beta z' I_{\boldsymbol{u},B(\mathbf{0})}(t)}\,\bigl(1 - e^{-z' H_{B(\mathbf{0}),t}}\bigr)\Bigr]\,\mathrm{d}z' \\
&= \int_0^\infty \frac{1}{1+z}\,\mathbb{E}\Bigl[e^{-\|X_{B(\mathbf{0})}-\boldsymbol{u}\|^\beta z I_{\boldsymbol{u},B(\mathbf{0})}(t)}\Bigr]\,\mathrm{d}z, \qquad (33)
\end{aligned}$$

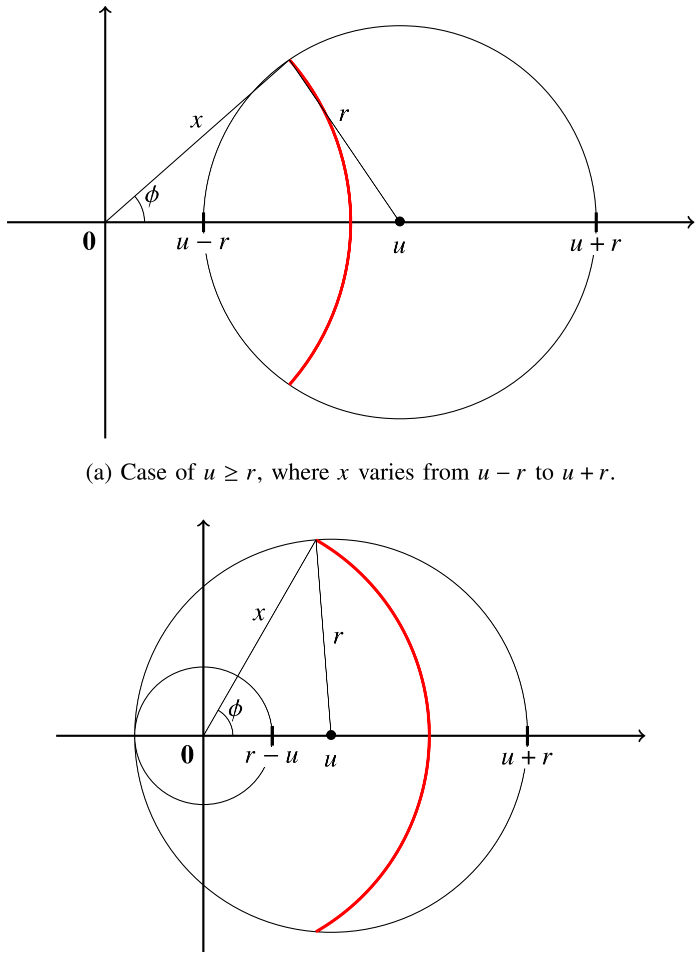

(a) Case of $u \geq r$, where x varies from $u - r$ to $u + r$.

(b) Case of $u < r$, where x varies from $r - u$ to $u + r$.

Fig. 9. Supplement to the derivation of eqs. (31) and (32), where $\phi = \arccos\Bigl(\dfrac{x^2 + u^2 - r^2}{2xu}\Bigr)$ for each $x \in [|u - r|, u + r]$.

where the second equality follows from $\mathbb{E}[e^{-z\,H_{B(\mathbf{0}),t}} \mid B(\mathbf{0})] = (1 + z)^{-1}$ because $H_{i,t}$, $i \in \mathbb{N}$, $t \in \mathbb{N}_0$, are mutually independent and exponentially distributed with unit mean. Furthermore, since $\|X_{B(\mathbf{0})}\|$ follows the probability density function $f_0(r) = 2\pi\lambda\, r e^{-\pi\lambda r^2}$ and the angle between $X_{B(\mathbf{0})}$ and $\boldsymbol{u}$ is uniformly distributed on $[0, 2\pi)$, the expectation in the last expression of (33) satisfies

$$\begin{aligned}
&\mathbb{E}\Bigl[e^{-\|X_{B(\mathbf{0})} - \boldsymbol{u}\|^{\beta}\, z\, I_{\boldsymbol{u},B(\mathbf{0})}(t)}\Bigr] \\
&= \frac{1}{2\pi}\int_0^{2\pi}\!\!\int_0^{\infty} \mathbb{E}\Bigl[e^{-{w_{r,u,\phi}}^{\beta}\, z\, I_{\boldsymbol{u},B(\mathbf{0})}(t)} \Bigm| \|X_{B(\mathbf{0})}\| = r\Bigr]\, f_0(r)\, \mathrm{d}r\, \mathrm{d}\phi \\
&\geq \lambda \int_0^{2\pi}\!\!\int_0^{\infty} r\, \exp\Bigl(-\pi\lambda r^2 - \pi\lambda\, K_\beta\, {w_{r,u,\phi}}^2\, z^{2/\beta}\Bigr)\, \mathrm{d}r\, \mathrm{d}\phi
\end{aligned}$$

$$= \lambda e^{-\pi\lambda K_\beta u^2 z^{2/\beta}} \int_0^{2\pi}\int_0^{\infty} r \,\exp\Bigl(-\pi\lambda\bigl[(1+K_\beta z^{2/\beta})\, r^2 - 2K_\beta\, u\, z^{2/\beta} r\cos\phi\bigr]\Bigr)\,\mathrm{d}r\,\mathrm{d}\phi$$

$$= \frac{1}{1+K_\beta z^{2/\beta}}\,\exp\Bigl(-\pi\lambda\, u^2\,\frac{K_\beta z^{2/\beta}}{1+K_\beta z^{2/\beta}}\Bigr), \tag{34}$$

where $w_{r,u,\phi} = \sqrt{r^2+u^2-2ru\cos\phi}$ and the inequality follows from (28), from which the nonnegative integral term is removed. In the last equality in (34), we apply the following; that is, for $p > 0$ and $q \in \mathbb{R}$,

$$\begin{aligned}\int_0^{2\pi}\int_0^{\infty} r\, e^{-p\, r^2+q\, r\cos\phi}\,\mathrm{d}r\,\mathrm{d}\phi &= \int_{-\infty}^{\infty}\int_{-\infty}^{\infty} e^{-p(x^2+y^2)+qx}\,\mathrm{d}x\,\mathrm{d}y\\ &= e^{q^2/(4p)}\int_{-\infty}^{\infty}\int_{-\infty}^{\infty} e^{-p(x^2+y^2)}\,\mathrm{d}x\,\mathrm{d}y\\ &= \frac{\pi}{p}\, e^{q^2/(4p)}.\end{aligned}$$

Finally, plugging (34) into (33) and changing the variables as $z' = K_\beta z^{2/\beta}$, we obtain (16).

Appendix D
Proof of Theorem 2

Following the discussion prior to Theorem 2, we approximately derive the length of the skipping period that maximizes the lower bound of the utility metric for sufficiently small moving speed of the typical UE. As in (17), let $\widetilde{\tau}$ denote the lower bound of τ given on the right-hand side of (16). As the first step of the approximation, we introduce continuous relaxation that considers s as a nonnegative real number though the skipping period essentially takes an integer in our discrete-time setting. Furthermore, we replace the sum in (9) with an integral. Namely, when the typical UE moves at constant speed v, the lower bound of the expected downlink data rate in (9) is approximated as

$$\widetilde{\mathcal{T}}(s) = \frac{1}{s}\int_0^{s} \widetilde{\tau}(tv)\,\mathrm{d}t, \tag{35}$$

which is now specified as a function of s. Similarly, when the moving speed of the typical UE is constant at v, the HO rate in (20) is reduced to

$$\mathcal{H}(s) = \frac{1}{s}\biggl[1 - 2\lambda\int_0^{\pi}\int_0^{\infty} r\, e^{-\lambda\,\eta(r,sv,\phi)}\,\mathrm{d}r\,\mathrm{d}\phi\biggr]. \tag{36}$$

We now consider the approximation of the lower bound of the utility metric defined as

$$\widetilde{\mathcal{U}}(s) = \widetilde{\mathcal{T}}(s) - c\,\mathcal{H}(s). \tag{37}$$

Our purpose is then to approximately derive the solution s of the equation that the following derivative is equal to 0;

$$\frac{\mathrm{d}\widetilde{\mathcal{U}}(s)}{\mathrm{d}s} = \frac{\mathrm{d}\widetilde{\mathcal{T}}(s)}{\mathrm{d}s} - c\,\frac{\mathrm{d}\mathcal{H}(s)}{\mathrm{d}s}. \tag{38}$$

Consider the first term $\mathrm{d}\widetilde{\mathcal{T}}(s)/\mathrm{d}s$ on the right-hand side of (38). From (35), we have

$$\frac{\mathrm{d}\widetilde{\mathcal{T}}(s)}{\mathrm{d}s} = \frac{1}{s}\,\widetilde{\tau}(sv) - \frac{1}{s^2}\int_0^s \widetilde{\tau}(tv)\,\mathrm{d}t. \tag{39}$$

Taylor's theorem applied to the exponential in $\widetilde{\tau}$ on the right-hand side of (16) leads to

$$\widetilde{\tau}(u) = \frac{\beta}{2}\int_0^\infty \frac{z^{\beta/2-1}}{(1+z)({K_\beta}^{\beta/2}+z^{\beta/2})}\Bigl(1 - \pi\lambda u^2\frac{z}{1+z}\Bigr)\,\mathrm{d}z + o(u^2) \quad \text{as } u \to 0.$$

Then, plugging this into (39), we have for sufficiently small $v > 0$,

$$\frac{\mathrm{d}\widetilde{\mathcal{T}}(s)}{\mathrm{d}s} \approx -\frac{\pi\lambda\beta}{3}\,sv^2\int_0^\infty \frac{z^{\beta/2}}{(1+z)^2({K_\beta}^{\beta/2}+z^{\beta/2})}\,\mathrm{d}z. \tag{40}$$

Next, to consider $\mathrm{d}\mathcal{H}(s)/\mathrm{d}s$ in (38), we take the derivative of the integrand on the right-hand side of (36); that is,

$$\frac{\partial}{\partial s} r\,e^{-\lambda\,\eta(r,sv,\phi)} = -\lambda r\,e^{-\lambda\,\eta(r,sv,\phi)}\,\frac{\partial}{\partial s}\eta(r,sv,\phi),$$

where (21) leads to

$$\frac{\partial}{\partial s}\eta(r,sv,\phi) = -2\,v\Bigl[(r\cos\phi - sv)\arccos\Bigl(\frac{r\cos\phi - sv}{w_{r,sv,\phi}}\Bigr) - r\sin\phi\Bigr],$$

with $w_{r,sv,\phi} = \sqrt{r^2 + (sv)^2 - 2\,rsv\cos\phi}$. By (21) and (22), we know that $\eta(r,sv,\phi) = \pi r^2 + |b_{\boldsymbol{y}}(w_{r,sv,\phi}) \setminus b_{\boldsymbol{0}}(r)| \ge \pi r^2$, so that,

$$\left|\frac{\partial}{\partial s} r\,e^{-\lambda\,\eta(r,sv,\phi)}\right| \le 2\lambda v e^{-\pi\lambda r^2}\,\bigl[(\pi+1)r^2 + \pi svr\bigr],$$

and for any fixed $s \in (0,\infty)$ and $v \in (0,\infty)$,

$$\int_0^\pi\!\!\int_0^\infty \left|\frac{\partial}{\partial s} r\,e^{-\lambda\,\eta(r,sv,\phi)}\right| \mathrm{d}r\,\mathrm{d}\phi \le \frac{(\pi+1)\,v}{2\lambda^{1/2}} + \pi sv^2 < \infty.$$

Therefore, we can change the order of the integral and derivative, and we have

$$\begin{aligned}\frac{\mathrm{d}\mathcal{H}(s)}{\mathrm{d}s} &= \frac{2\lambda^2}{s}\int_0^\pi\!\!\int_0^\infty r\,e^{-\lambda\,\eta(r,sv,\phi)}\,\frac{\partial}{\partial s}\eta(r,sv,\phi)\,\mathrm{d}r\,\mathrm{d}\phi \\ &\quad - \frac{1}{s^2}\Bigl\{1 - 2\lambda\int_0^\pi\!\!\int_0^\infty r\,e^{-\lambda\,\eta(r,sv,\phi)}\,\mathrm{d}r\,\mathrm{d}\phi\Bigr\} \\ &= \frac{2\lambda}{s}\int_0^\pi\!\!\int_0^\infty r\,e^{-\lambda\,\eta(r,sv,\phi)}\Bigl(\lambda\,\frac{\partial}{\partial s}\eta(r,sv,\phi) + \frac{1}{s}\Bigr)\,\mathrm{d}r\,\mathrm{d}\phi - \frac{1}{s^2}.\end{aligned} \tag{41}$$

Taylor's theorem applied to the integrand above gives

$$\begin{aligned}
&r\, e^{-\lambda\,\eta(r,sv,\phi)} \left(\lambda\, \frac{\partial}{\partial s}\eta(r,sv,\phi) + \frac{1}{s}\right) \\
&= r\, e^{-\pi\lambda r^2} \left\{\frac{1}{s} - \lambda s v^2 \bigl[2\lambda r^2(\phi\cos\phi - \sin\phi)^2 - \phi + \cos\phi\sin\phi\bigr]\right\} + o(v^2) \quad \text{as } v \to 0,
\end{aligned}$$

and we have for sufficiently small $v > 0$,

$$\begin{aligned}
\frac{\mathrm{d}\mathcal{H}(s)}{\mathrm{d}s} &\approx \frac{2\lambda}{s}\int_0^{\pi}\!\!\int_0^{\infty} r\, e^{-\pi\lambda r^2} \left\{\frac{1}{s} - \lambda s v^2 \bigl[2\lambda r^2(\phi\cos\phi - \sin\phi)^2 - \phi + \cos\phi\sin\phi\bigr]\right\} \mathrm{d}r\, \mathrm{d}\phi - \frac{1}{s^2} \\
&= -\Bigl(\frac{5}{2\pi} - \frac{\pi}{6}\Bigr)\lambda\, v^2. \qquad (42)
\end{aligned}$$

Hence, plugging (40) and (42) into (38) derives

$$\frac{\mathrm{d}\widetilde{\mathcal{U}}(s)}{\mathrm{d}s} \approx -\frac{\pi\lambda\beta}{3}\, s v^2 \int_0^{\infty} \frac{z^{\beta/2}}{(1+z)^2({K_\beta}^{\beta/2} + z^{\beta/2})}\, \mathrm{d}z + \Bigl(\frac{5}{2\pi} - \frac{\pi}{6}\Bigr) c\, \lambda\, v^2.$$

The right-hand side above is linearly decreasing in s, and solving the equation that it is equal to 0 with respect to s, we obtain (24).

References

[1] K. Tokuyama and N. Miyoshi, "Data rate and handoff rate analysis for user mobility in cellular networks," in *2018 IEEE Wireless Communications and Networking Conference (WCNC)*, Barcelona, Spain, April 2018.

[2] N. Bhushan, J. Li, D. Malladi, R. Gilmore, D. Brenner, A. Damnjanovic, R. T. Sukhavasi, C. Patel, and S. Geirhofer, "Network densification: The dominant theme for wireless evolution into 5G," *IEEE Communications Magazine*, vol. 52, no. 2, pp. 82–89, February 2014.

[3] M. Kamel, W. Hamouda, and A. Youssef, "Ultra-dense networks: A survey," *IEEE Communications Surveys & Tutorials*, vol. 18, no. 4, pp. 2522–2545, Fourthquarter 2016.

[4] R. Arshad, H. ElSawy, S. Sorour, T. Y. Al-Naffouri, and M.-S. Alouini, "Handover management in dense cellular networks: A stochastic geometry approach," in *2016 IEEE International Conference on Communications (ICC)*, Kuala Lumpur, May 2016.

[5] ——, "Velocity-aware handover management in two-tier cellular networks," *IEEE Transactions on Wireless Communications*, vol. 16, no. 3, pp. 1851–1867, March 2017.

[6] ——, "Cooperative handover management in dense cellular networks," in *2016 IEEE Global Communications Conference (GLOBECOM)*, Washington DC, December 2016.

[7] ——, "Handover management in 5G and beyond: A topology aware skipping approach," *IEEE Access*, vol. 4, pp. 9073–9081, December 2016.

[8] E. Demarchou, C. Psomas, and I. Krikidis, "Mobility management in ultra-dense networks: Handover skipping techniques," *IEEE Access*, vol. 6, pp. 11 921–11 930, February 2018.

[9] X. Wu and H. Haas, "Handover skipping for LiFi," *IEEE Access*, vol. 7, pp. 38 369–38 378, March 2019.

[10] C. Suarez-Rodriguez, Y. He, B. A. Jayawickrama, and E. Dutkiewicz, "Low-overhead handover-skipping technique for 5G networks," in *2019 IEEE Wireless Communications and Networking Conference (WCNC)*, Marrakesh, April 2019.

[11] H. ElSawy, A. Sultan-Salem, M.-S. Alouini, and M. Z. Win, “Modeling and analysis of cellular networks using stochastic geometry: A tutorial,” *IEEE Communications Surveys & Tutorials*, vol. 19, no. 1, pp. 167–203, Firstquarter 2017.

[12] H. Tabassum, M. Salehi, and E. Hossain, “Fundamentals of mobility-aware performance characterization of cellular networks: A tutorial,” *IEEE Communications Surveys & Tutorials*, vol. 21, no. 3, pp. 2288–2308, Thirdquarter 2019.

[13] F. Baccelli and S. Zuyev, “Stochastic geometry models of mobile communication networks,” in *Frontiers in Queueing: Models and Applications in Science and Engineering*, J. H. Dshalalow, Ed. Boca Raton: CRC Press, 1997, ch. 8, pp. 227–243.

[14] F. Baccelli, M. Klein, M. Lebourges, and S. Zuyev, “Stochastic geometry and architecture of communication networks,” *Telecommunications Systems*, vol. 7, no. 1–3, pp. 209–227, June 1997.

[15] X. Lin, R. K. Ganti, P. J. Fleming, and J. G. Andrews, “Towards understanding the fundamentals of mobility in cellular networks,” *IEEE Transactions on Wireless Communications*, vol. 12, no. 4, pp. 1686–1698, April 2013.

[16] Y. Hong, X. Xu, M. Tao, J. Li, and T. Svensson, “Cross-tier handover analyses in small cell networks: A stochastic geometry approach,” in *2015 IEEE International Conference on Communications (ICC)*, London, June 2015, pp. 3429–3434.

[17] W. Bao and B. Liang, “Stochastic geometric analysis of user mobility in heterogeneous wireless networks,” *IEEE Journal on Selected Areas in Communications*, vol. 33, no. 10, pp. 2212–2225, October 2015.

[18] ——, “Stochastic geometric analysis of handoffs in user-centric cooperative wireless networks,” in *IEEE INFOCOM 2016—The 35th Annual IEEE International Conference on Computer Communications*, San Fransisco, CA, April 2016.

[19] S. Sadr and R. S. Adve, “Handoff rate and coverage analysis in multi-tier heterogeneous networks,” *IEEE Transactions on Wireless Communications*, vol. 14, no. 5, pp. 2626–2638, May 2015.

[20] A. Chattopadhyay, B. Błaszczyszyn, and E. Altman, “Two-tier cellular networks for throughput maximization of static and mobile users,” *IEEE Transactions on Wireless Communications*, vol. 18, no. 2, pp. 997–1010, February 2019.

[21] J. G. Andrews, F. Baccelli, and R. K. Ganti, “A tractable approach to coverage and rate in cellular networks,” *IEEE Transactions on Communications*, vol. 59, no. 11, pp. 3122–3134, November 2011.

[22] B. Błaszczyszyn, M. Haenggi, P. Keeler, and S. Mukherjee, *Stochastic Geometry Analysis of Cellular Networks*. Cambridge: Cambridge University Press, 2018.

[23] S. N. Chiu, D. Stoyan, W. S. Kendall, and J. Mecke, *Stochastic Geometry and its Applications*, 3rd ed. Chichester: Wiley, 2013.

[24] 3GPP, “Evolved universal terrestrial radio access (E-UTRA); radio resource control (RRC); protocol specification,” 3rd Generation Partnership Project (3GPP), Technical Specification (TS) 36.331, March 2020, v16.0.0.

[25] H. Q. Nguyen, F. Baccelli, and D. Kofman, “A stochastic geometry analysis of dense IEEE 802.11 networks,” in *IEEE INFOCOM 2007—26th IEEE International Conference on Computer Communications*, Anchorage, AK, May 2007, pp. 1199–1207.

[26] J. Møller, “Random tessellations in $\mathbb{R}^d$,” *Advances in Applied Probability*, vol. 21, no. 1, pp. 37–73, March 1989.

[27] F. Baccelli and S. Zuyev, “Poisson-voronoi spanning trees with applications to the optimization of communication networks,” *Operations Research*, vol. 47, no. 4, pp. 619–631, July–August 1999.

[28] Y. Xu, K. Tokuyama, and Y. Wada, “Handover skipping analysis in dense cellular network using Poisson cluster process,” in *2022 IEEE 95th Vehicular Technology Conference (VTC2022-Spring)*, Helsinki, June 2022.

[29] K. A. Hamdi, “A useful lemma for capacity analysis of fading interference channels,” *IEEE Transactions on Communications*, vol. 58, no. 2, pp. 411–416, February 2010.

[30] D. J. Daley and D. Vere-Jones, *An Introduction to the Theory of Point Processes: Volume II: General Theory and Structure*, 2nd ed. New York, NY: Springer, 2008.